China Geology 7 (2024) 36−50

China Geology

Journal homepage: http://chinageology.cgs.cn
https://www.sciencedirect.com/journal/china-geology

Deep-large faults controlling on the distribution of the venting gas hydrate system in the middle of the Qiongdongnan Basin, South China Sea

Jin-feng Ren[a, b], Hai-jun Qiu[c,*], Zeng-gui Kuang[b], Ting-wei Li[b], Yu-lin He[b], Meng-jie Xu[b], Xiao-xue Wang[b], Hong-fei Lai[b], Jin Liang[b]

[a] *National Engineering Research Center of Gas Hydrate Exploration and Development*, *Guangzhou* 511458, *China*
[b] *Guangzhou Marine Geological Survey*, *China Geological Survey*, *Guangzhou* 511458, *China*
[c] *China Geological Survey*, *Ministtry of Natural Resources*, *Beijing* 100037, *China*

ARTICLE INFO

Article history:
Received 30 March 2023
Received in revised form 7 August 2023
Accepted 7 October 2023
Available online 13 January 2024

Keywords:
Venting gas hydrates
Deep-large faults
Gas chimney
Gas-escape pipes
High-resolution 3D seismic
Logging while drilling
Qiongdongnan Basin
South China Sea

ABSTRACT

Many locations with concentrated hydrates at vents have confirmed the presence of abundant thermogenic gas in the middle of the Qiongdongnan Basin (QDNB). However, the impact of deep structures on gas-bearing fluids migration and gas hydrates distribution in tectonically inactive regions is still unclear. In this study, the authors apply high-resolution 3D seismic and logging while drilling (LWD) data from the middle of the QDNB to investigate the influence of deep-large faults on gas chimneys and preferred gas-escape pipes. The findings reveal the following: (1) Two significant deep-large faults, F1 and F2, developed on the edge of the Songnan Low Uplift, control the dominant migration of thermogenic hydrocarbons and determine the initial locations of gas chimneys. (2) The formation of gas chimneys is likely related to fault activation and reactivation. Gas chimney 1 is primarily arises from convergent fluid migration resulting from the intersection of the two faults, while the gas chimney 2 benefits from a steeper fault plane and shorter migration distance of fault F2. (3) Most gas-escape pipes are situated near the apex of the two faults. Their reactivations facilitate free gas flow into the GHSZ and contribute to the formation of fracture - filling hydrates.

1. Introduction

Gas hydrates are ice-like compounds composed of a gas molecule encased in a water lattice (Sloan ED and Koh C, 2007). The most common gas molecule in nature is methane (Kvenvolden KA, 1995; Boswell R and Collett TS, 2011). One volume of methane hydrate can release approximately 160–180 volumes of methane under standard temperature and pressure conditions (Sloan ED, 2003; Collett TS et al., 2009). Gas hydrates encapsulate a significant portion of the organic carbon (Boswell R and Collett TS, 2011; Milkov AV, 2004). These attributes position gas hydrates as an efficient and relatively-cleaner energy, ranking among the most abundant unconventional energy resources in the world (Collett TS, 2004; Burwicz E et al., 2011; Boswell R and Collett TS, 2011; Koh DY et al., 2016).

Submarine continental margins with water depths exceeding 350–600 m provide suitable conditions for gas hydrate accumulations. However, concentrated gas hydrates are not common within typical continental margin sediments (Boswell R and Collett TS, 2011). The formation of gas hydrate likely occurs at low concentrations (<10% of sediment pore space) and in local by the microbial biodegradation (Malinverno A, 2010; Wallmann K et al., 2012). Therefore, understanding the mechanisms governing gas migration in a long distance from deep strata and the formation of concentrated gas hydrates is critical for the exploration of subsea gas hydrate resources.

Concentrated hydrates at vent systems are widespread in submarine continental margins (You KY et al., 2019). Scientific drilling has revealed gas hydrate concentrations ranging from 40% to >90% in various vent locations, such as (1) the eastern margin of the Japan Sea (Matsumoto R et al., 2017), (2) the Ulleung Basin, South Korea (Lee MW and

First author: *E-mail address*: jf_ren@163.com (Jin-feng Ren).
* Corresponding author: *E-mail address*: gmgs_qiu@sina.com (Hai-jun Qiu).

Literary editor: Li-qiong Jia
doi:10.31035/cg2023086
2096-5192/© 2024 China Geology Editorial Office.

Collett TS, 2013; Ryu BJ et al., 2013), (3) the southern summit of Hydrate Ridge, Cascadia Margin (Torres ME et al., 2004; Trèhu, AM et al., 2004), and (4) the northern slope of the South China Sea (Sha ZB et al., 2015; Ye JL et al., 2019; Zhang W et al., 2020; Liang JQ et al., 2021). In some of these systems, concentrated hydrates fill fractures in muddy sediments with vents often penetrating the gas hydrate stability zone (GHSZ). Pockmarks, carbonate deposits, massive gas hydrate, and chemosynthetic communities are present near the seafloor.

Freire AFM et al. (2011) reported that a combination of faults, anticline shape, and carrier beds induced thermogenic gas migration toward the top of the structure, delivering gas through the GHSZ. Strong venting resulted in excess gas flux reaching the seafloor in the eastern margin of Japan Sea. Yoo DG et al. (2017) also reported that fault and fracture systems associated with seismic chimneys played an important role in the upward migration of fluid or gas originating from below the GHSZ in the Ulleung Basin. Numerical modeling by Dhakal S and Gupta I (2021) suggested that gas hydrates in the Southern Hydrate Ridge could form from gas migrating along faults from deeper sources. Liang JQ et al. (2021) proposed a model of gas hydrate accumulation controlled by the gas chimney, which transported the deep hydrocarbons to the GHSZ, resulting in gas hydrate formation and gas accumulation in the Qiongdongnan Basin (QDNB). Thus, vented gas is most likely be supplied from the crest of permeable pathways beneath the GHSZ, such as fractured or faulted systems, dipping sand bodies, gas chimney and within anticlinal structures (Paganoni M et al., 2018; Berndt C et al., 2019; Liang JQ et al., 2019; Santra et al., 2022).

The QDNB is a key exploration area on the northern slope of the South China Sea (SCS), known for its extremely rich in gas hydrate and hydrocarbon resources (Zhu JT et al., 2020; He JX et al., 2022; Ren JF et al., 2022). In recent years, geological and geophysical markers, including bottom simulating reflection (BSR), and anomalies associated with the occurrence of fracture-filling gas hydrates were found in the Songnan and Lingnan Low Uplifts (Zhang W et al., 2020; He YL et al., 2022). In 2015, an active cold seep was discovered by a remotely operated vehicle (ROV) in the Haima Cold Seep, the Lingnan Low Uplift. Massive gas hydrate samples from shallow sediments were obtained by gravity piston cores (Liang QY et al., 2017). In 2018, the Guangzhou Marine Geological Survey (GMGS) conducted a gas hydrate drilling expedition including logging while drilling (LWD) operations at five locations and coring operations at three locations to assess the geologic occurrence of concentrated gas hydrates at vents in the Songnan Low Uplift of QDNB. The results revealed the presence of massive, layered, nodular, fracture-filling, and dispersed gas hydrates at the top of the three gas chimneys. Molecular and isotopic analyses indicated that the source gas originated from both of the thermogenic and microbial gas and may have degraded gas during migration from a deep source (Ye JL et al., 2019; Lai HF et al., 2021).

In this paper, the authors present three-dimensional (3-D) seismic and LWD data to analyze the influences of fault system and gas chimney on the distribution of natural gas hydrate in the low uplift area. This study addresses the following questions: (1) How does the deep fault influence the deep-seated dominant migration pathways and subsequent gas chimney formation? (2) Are there relationships between the fault system and concentrated hydrate in gas-escape pipes?

2. Geological setting

The QDNB is located at the western end of the extensional rifted continental margin in the northern SCS, between the Hainan Island and Xisha Islands (Fig. 1a). It is a Cenozoic intra-continental rifted basin developed on the pre-Cenozoic basement. From north to south, QDNB is divided into northern depression belt, northern uplift belt, central depression belt and southern uplift belt (Song P et al., 2021). The central depression belt is divided into eastern and western parts by the Songnan Low Uplift. The western part is composed of the Ledong Sag and Lingshui Sag, oriented in a northeast-southwest direction, whereas the eastern part is composed of the Songnan-Baodao Sag and Changchang Sag, which are aligned in an east-west direction (Fig. 1b). Consequently, the Songnan Low Uplift is located in the structural transition zone in the center of QDNB, serving as a key exploration area for gas hydrate (Fig. 1c).

2.1. Tectonic, stratigraphic, and sedimentary evolution

Zhang CM et al. (2013) reported the spatial and temporal distribution of regional syn-sedimentary faults of four periods developed in the QDNB, (1) NE-trending faults of the basement, (2) E-W-trending faults in the westernmost QDNB and NE-trending faults in the middle and east of QDNB at around 36 Ma, (3) E-W- and NE-trending faults of the western and the middle basin and NW- and E-W-trending faults of the eastern basin at around 30 Ma, and (4) most faulting stopped 21 Ma, with the exception of some E-W- and NW-trending faults within the middle and the eastern basin. Mao KN et al. (2015) observed that the basement fault systems were reactivated after the Late Miocene (11.6 Ma), creating a small sub-basin characterized by distinctive axial negative topography.

Through the identification and tracking of seismic stratigraphic boundaries, the authors observed an apparent angular unconformity and semi-parallel seismic reflections underneath the Cenozoic basement. This suggests that the pre-Cenozoic strata may have been developed on the Songnan Low Uplift but subsequently subjected to intense erosion (Fig. 2). These strata underwent complex tectonic deformation, potentially influenced by Cenozoic tectonic activity and late magmatic diapir intrusion.

Since Cenozoic, the tectonic activity of the Songnan Low Uplift has been synchronized with the whole tectonic movement of QDNB (Fig. 2). The Eocene-Early Oligocene (Tg-T70) marks the regional rifting stage. During this period, the low uplift began to develop and deposited the Eocene lacustrine facies and the Lower Oligocene marine-continental

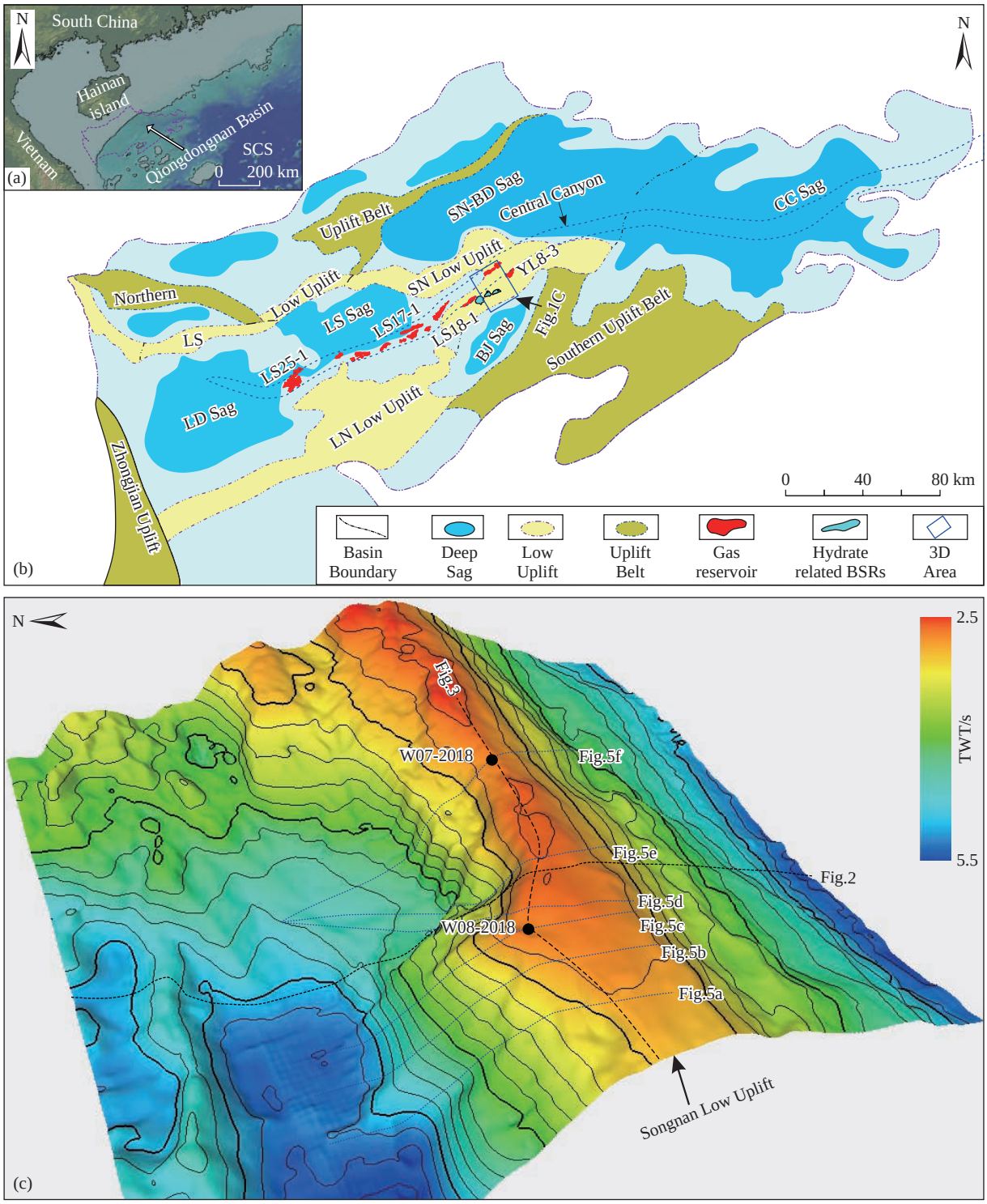

Fig. 1. a–Regional map of the northwestern South China Sea showing the locations of the Qiongdongnan Basin. SCS-South China Sea, LD-Ledong, LS-Lingshui, LN-Lingnan, BJ-Beijiao, SN-Songnan, BD-Baodao, CC-Changchang. b–Structure map of Qiongdongnan Basin showing the locations of hydrate-related BSRs (after Deng W et al., 2021), gas fields (LS25-1, LS17-2, LS18-1, and YL8-3) (after Xiong XF et al., 2019) and the study area. c–3D visualization of the Cenozoic basement surface interpreted based on the seismic reflection data, showing the depth structural features and the outlines of Songnan Low Uplift of the study area. Also showing the locations of Figs. 2, 3, and 5 and Sites W08-2018 and W07-2018.

transitional facies, which serve as the primary source rocks of QDNB. In the Late Oligocene (T70-T60), the area entered a fault-depression stage. The eastern and western sides of the Central Depression belt started to diverge, leading to the development of numerous nearly EW-trending faults. Additionally, early NE-trending faults inherited oblique extension around the periphery of the low uplift, receiving coastal facies and shallow marine facies deposits.

Simultaneously, due to the intrusion of magmatic diapir, the initially deposited strata underwent tectonic uplifting during this period, further elevating the low uplift. During the Miocene (T60-T40), QDNB entered a post-rifting thermal

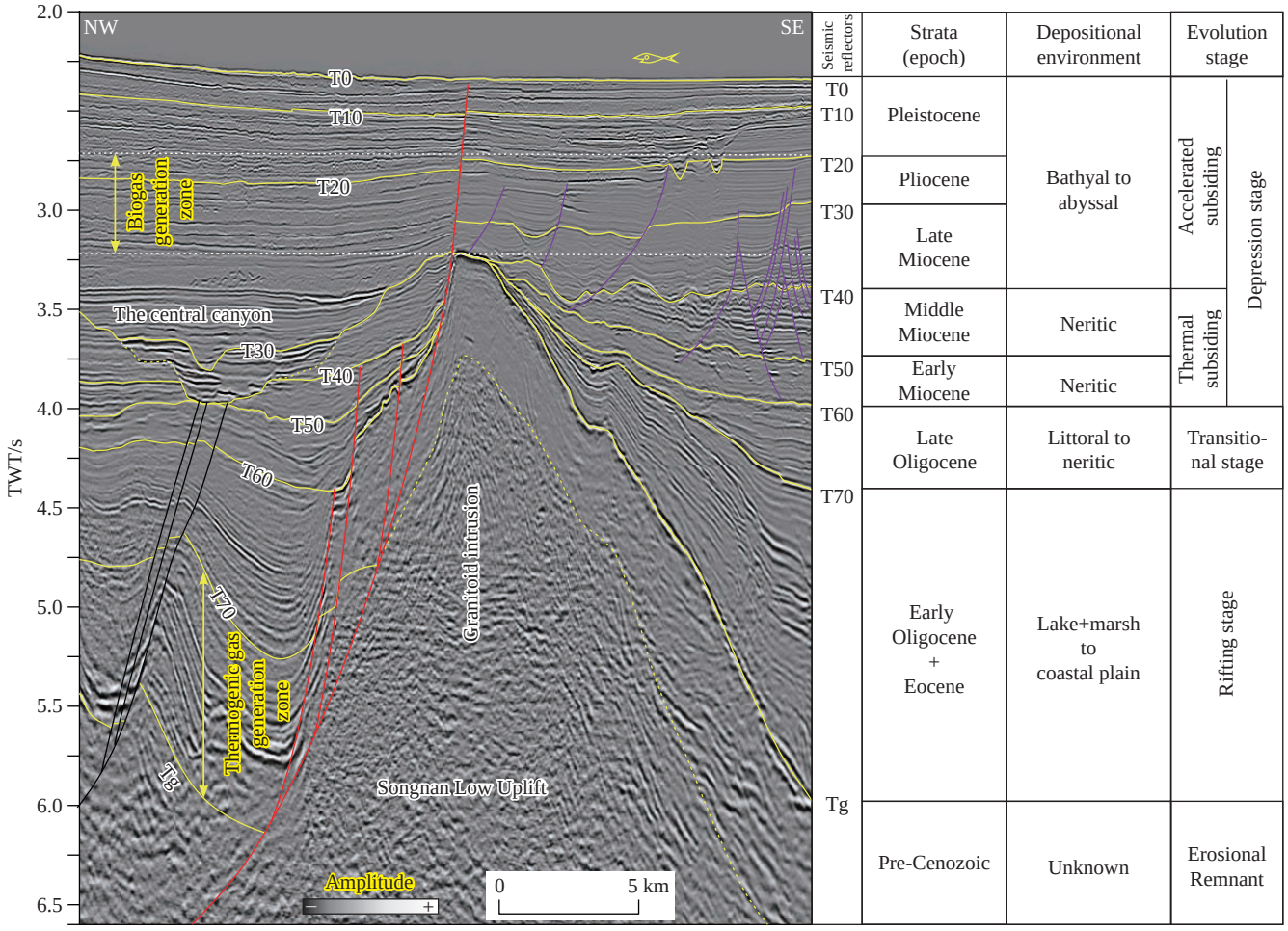

Fig. 2. Interpreted seismic section (left) (see the location in Fig. 1) passing the Songnan Low Uplift displaying biogas generation zone and thermogenic gas generation zone in the study area and composite stratigraphic column (right) showing the tectonic evolution and depositionnal environment of the Qiongdongnan Basin. The yelow curves are stratigraphic surfaces. The black lines are deep-seated faults that are mainly active in the rifting stage. The red lines are deep-large faults that are active from deep sag to near seabed. The purple lines are polygonal and post-depositional faults.

subsiding stage. The periphery of the low uplift received continuous deposition, progressing from shore-shallow marine facies to semi-deep Marine facies. In the Late Miocene (T40-T30), a large-scale central canyon gradually formed across the Central Depression belt. Moving to the Late Miocene-Pliocene (T40-T20), the low uplift began to experience flooding, accumulating stable fine-grained semi-abyssal to abyssal muddy deposits and mass transport deposits. In the Early Quaternary (T20-T10), deep-water channel-levee deposits from the western part of the basin began to develop crossing the low uplift area. In the Late Quaternary (T10-T0 (seabed)), three mass transport complex were predominantly developed in this study area.

2.2. Petroleum system in the Songnan Low Uplift

The Songnan Low Uplift area serves as a common enrichment region for both the deep hydrocarbon system and shallow gas hydrate system. Two types of gas-bearing trap reservoirs have been discovered. The first type is lithologic trap reservoirs (such as LS17-2, LS8-1, and LS18-2), primarily composed of channel turbiditic sandstones developed in the Central Canyon (Shi HS et al., 2019). The second type is structural trap reservoirs, mainly composed of pre-Cenozoic igneous fractured reservoirs on top of the low uplift (Xu SL et al., 2019). The source gas for these reservoirs predominantly originate from coal-bearing source rocks in the Early Oligocene transitional facies (Zhang YZ et al., 2019a, 2019b).

The first type of fluid migration primarily involves vertical migration along high-angle faults, mud diapirs, and fractures along the canyon bottom (Fig. 2). In contrast, the second type of the fluid migration is mainly the lateral migration along low-angle regional faults, structural ridges, and inclined sand layers. Since the Miocene, strong hydrocarbon generation and widespread fluid activity have resulted in a wide distribution of gas chimneys. For example, the L25-1 gas field at the north side of the low uplift experienced two charging stages, namely 2.0 Ma mature-high mature gas charging and the near-present high mature gas charging (Zhang YZ et al., 2019a).

2.3. Gas hydrate system in the Songnan Low Uplift

Seismic interpretation has identified three favorable areas

of leakage type hydrate systems on the Songnan Low Uplift. These findings have been further confirmed by the LWD and sample coring expedition. A complex gas hydrate system within a gas chimney has been established in the Site W08. Authigenic carbonate concretions of different thickness (at depths of 3 mbsf and 52.1–53.6 mbsf) at vent sites indicate recurrent activity of cold seeps (Ye JL et al., 2019).

The presence of heavier hydrocarbons (C_2+(2.31%–18.79 %)) and sII gas hydrate in the Site W08-2018 indicates C_2+ hydrocarbon gases within the gas hydrates are typical thermogenic gas originating from deeply buried coaly-type gas pools or source rocks (Lai HF et al., 2020; Wei JG et al., 2021). Thermogenic gases were probably both supplied by thermogenic gas source rocks in the Early Oligocene coal-bearing deposits and biogenic gas source rocks in the Late Miocene–Pliocene argillaceous deposits with depths of 2150–2750 m (Fig. 2; Liang JQ et al., 2019; Lai HF et al., 2020).

Gas chimneys on the Songnan Low Uplift are interpreted as the primary pathways of gas-bearing fluids (Wei JG et al., 2021). The distribution thickness, occurrence and saturation of gas hydrates exhibit noticeable heterogeneity. These hydrates are mainly distributed within the gas-escape pipes, with only thin layers of hydrates accumulating in the area without pipes. Fracture-filling hydrates were recovered in high-angle fractures developed in the fine-grained clay-silt sediments of shallow mass transport deposits (MTDs) (Deng W et al., 2020).

3. Data and methods

A pseudo-3D seismic data utilized in this study were acquired in 2018 and 2020 in the Songnan Low Uplift area of the QDNB by the GMGS. The pseudo-3D survey consists of dense 2D lines covering a region of 400 km^2, at water depths between 1650 m and 1800 m. Seismic records with a 8s duration were acquired at 1 ms sampling rate. The raw data exhibited a frequency range of 6–200 Hz, with a vertical resolution of approximately 10 m. The processing bin size was 25 m × 6.25 m, and the velocity spectrum was analyzed at intervals of 250 m × 150 m. The seismic data was processed to zero phase and was displayed in reversed polarity according to SEG standard.

Deep faults, gas chimneys, and key horizons were interpreted using the GeoFrame 2012 Software Platform. In this study, a greyscale color bar is used to emphasize faults, gas chimneys and gas-escape pipes. A black-white color bar is used in seismic section, highlighting the strongest peaks in white and the strongest troughs in black, effectively representing differences between “low” and “high” values (Fig. 2). Variance time-slice maps extracted from seismic cube played a crucial role in detecting anomalies associated with low uplift, faults, gas chimneys, and gas-escape pipes.

Sites W07-2018 and W08-2018 was chosen to drill through two localized vertical pipes of gas venting interpreted from seismic profiles (Fig. 3). These pipe-like structures are referred to as gas-venting pipes in this study. These sites were drilled by GMGS using Schlumberger LWD tools. The available LWD data mainly included caliper, natural gamma rays, resistivity, neutron density, neutron porosity, velocity, and nuclear magnetic resonance data. These data with penetration depths up to 200 mbsf were collected to analyze the presence of gas hydrate and free gas. Higher resistivity and velocity anomalies indicate the occurrence of gas hydrate. Higher density may be caused by the presence of carbonate concretions. Higher resistivity and hole enlargement anomalies result from free gas in the sand layer. The distribution range of gas hydrate was delineated through the synthetic records of seismic and well logging, along with their comprehensive analysis.

4. Results and interpretations

4.1. Songnan Low Uplift

The 3D Time-Depth structural map of the Cenozoic basement (Tg) and the variance horizontal slice of 3500 ms from the variance cube reveal the low uplift with northeastward distribution (Fig. 4a). An angular unconformity with distinctive truncation was observed on the Tg boundary in the Beijiao Sag, and layered pre-Cenozoic strata and high-angle fracture zone were identified on the Songnan Low Uplift (Fig. 5). Compared to the distribution of pre-Cenozoic strata in other places of the northern South China Sea, the authors inferred that eroded remnants of sedimentary strata were developed on the upper low uplift. Geologic structural interpretation of typical seismic profiles further enables the division of formation and evolution of the low uplift into three stages.

The first stage corresponds the initial formation period, occurring during the rifting stage of the basin. Influenced by regional extensional tectonism, shallow-water lacustrine deposits with onlap termination likely developed on the low uplift. The second stage marks the rapid uplift period, during which the pre-Cenozoic strata of the low uplift underwent severe flexural deformation and formed a fracture-compartmentalized anticline due to the magma intrusion. The third stage encompasses the submergence period. The low uplift began to suffer denudation and gradually submerges. Fine-grained abyssal argillaceous deposits began to accumulate on the top of the low uplift. The stereogram of the Tg surface shows a vertical height difference of 2500–3500 m between the top of the low uplift and the eastern Lingshui Sag (Fig.1c). In particular, the thickness of the Late Miocene-Pliocene strata in the uplift area was obviously different from that in the sag area, suggesting a potential influence of differential subsidence due to accelerated regional subsidence in the basin.

4.2. Deep-large faults in the uplift margin

Two deep-large fault systems in the northwestern edge of Songnan Low Uplift were identified by the detailed interpretation of seismic profiles and horizontal variance

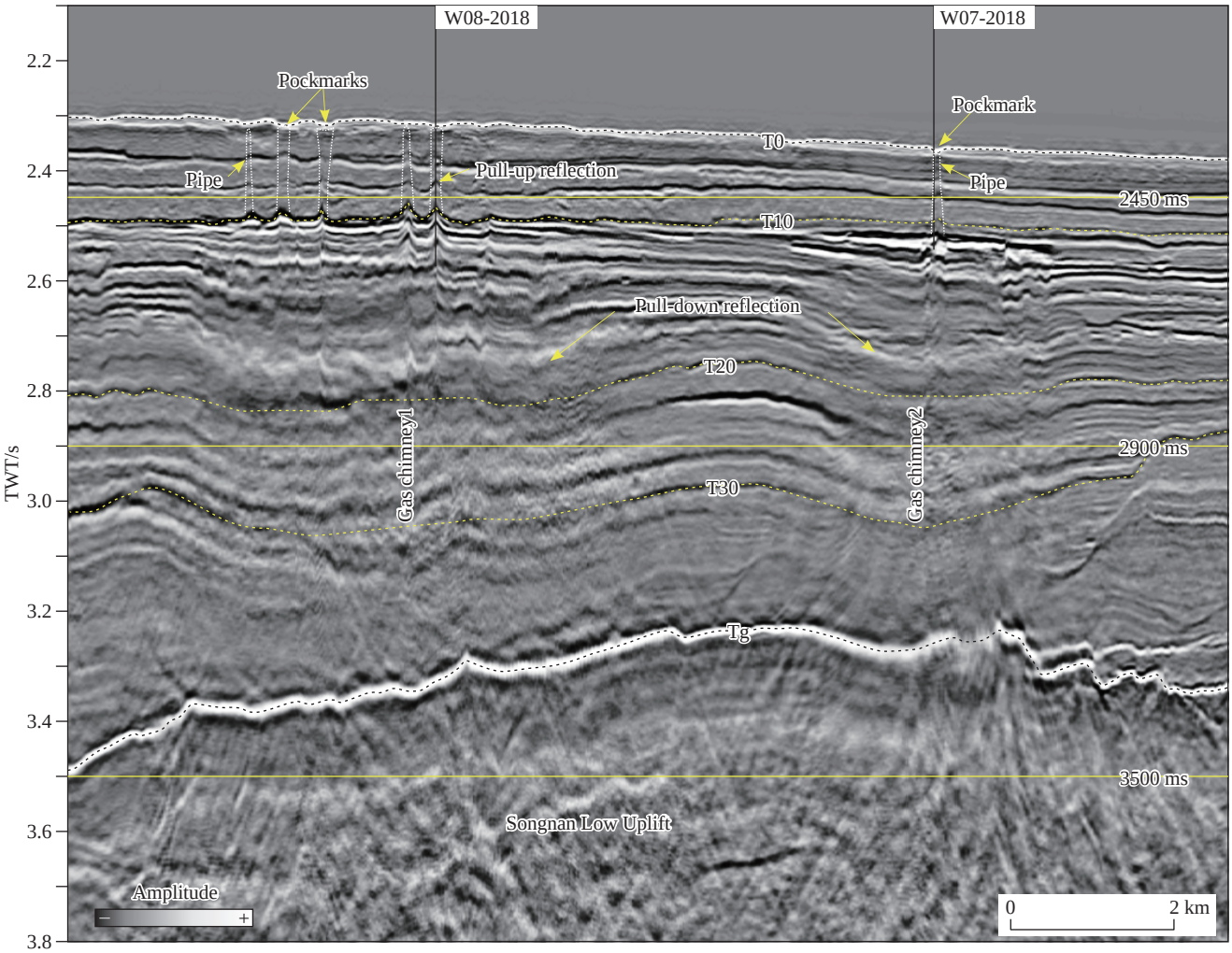

Fig. 3. Seismic profile traverse passing through sites W07-2018 and W08-2018 (see the location in Fig. 1c) in the study area displaying gas chimneys, gas-escapae pipes and pockmarks.

slices (Figs. 4, 5). The first fault, F1, exhibits a linear distribution on the plane with a strike of NE trending and an extending length of about 4.2 km. The second fault, F2, show an arc distribution on the plane, in which the strike of the western section is NW, and the strike of the eastern section is NEE, with an extending length of about 4.5 km (Fig. 5). Vertically, these fault systems have a Y-shaped characteristic, which may be related to the integrated effects of extension and strike-slip within the structural transition zone in the study area.

These faults extend into the basement of Cenozoic sedimentary basins and remain active in close proximity to the seafloor. Combined with tectonic and sedimentary evolution of QDNB, their tectonic activities also can be divided into four stages (Figs. 2, 5):

(i) The first phase occurred in the rifting period, and faults began to move under the influence of regional extension. This resulted in the development of a graben in the eastern Lingshui sub-sag and half graben in the Beijiao Sag.

(ii) The second phase occurred during the rifting-depression transition period. With the intrusion of a magma body into the footwall of the fault, the low uplift experienced rapid ascent, leading to intensified fault activity and significant fault displacement. At the same time, the Eocene-Early Oligocene sedimentary strata of the Beijiao Sag underwent structural tilting and the top of the low uplift emerged above the sea level, undergoing erosion.

(iii) The third stage occurred in the thermal subsiding stage. While the faults continued to move, their activity rate decreased, and in some cases, even came to a halt.

(iv) The fourth stage transpired during an accelerated subsiding period. Because of the great difference in subsidence rate between the deep sag area and the low uplift area, the fault inherited reactivities. The development of canyon channel and large-scale mass-transport complexes in the early stage led to distinctive growth patterns in the sedimentary strata on either side of the faults. The hanging wall of the fault primarily comprised sediments of alternative mass-transport complexes and deep-water turbidity currents, while the footwall was dominated by fine-grained deep-water muddy deposits.

4.3. Gas chimney

Gas chimneys exhibit distinct seismic signatures characterized by disrupted reflections, commonly

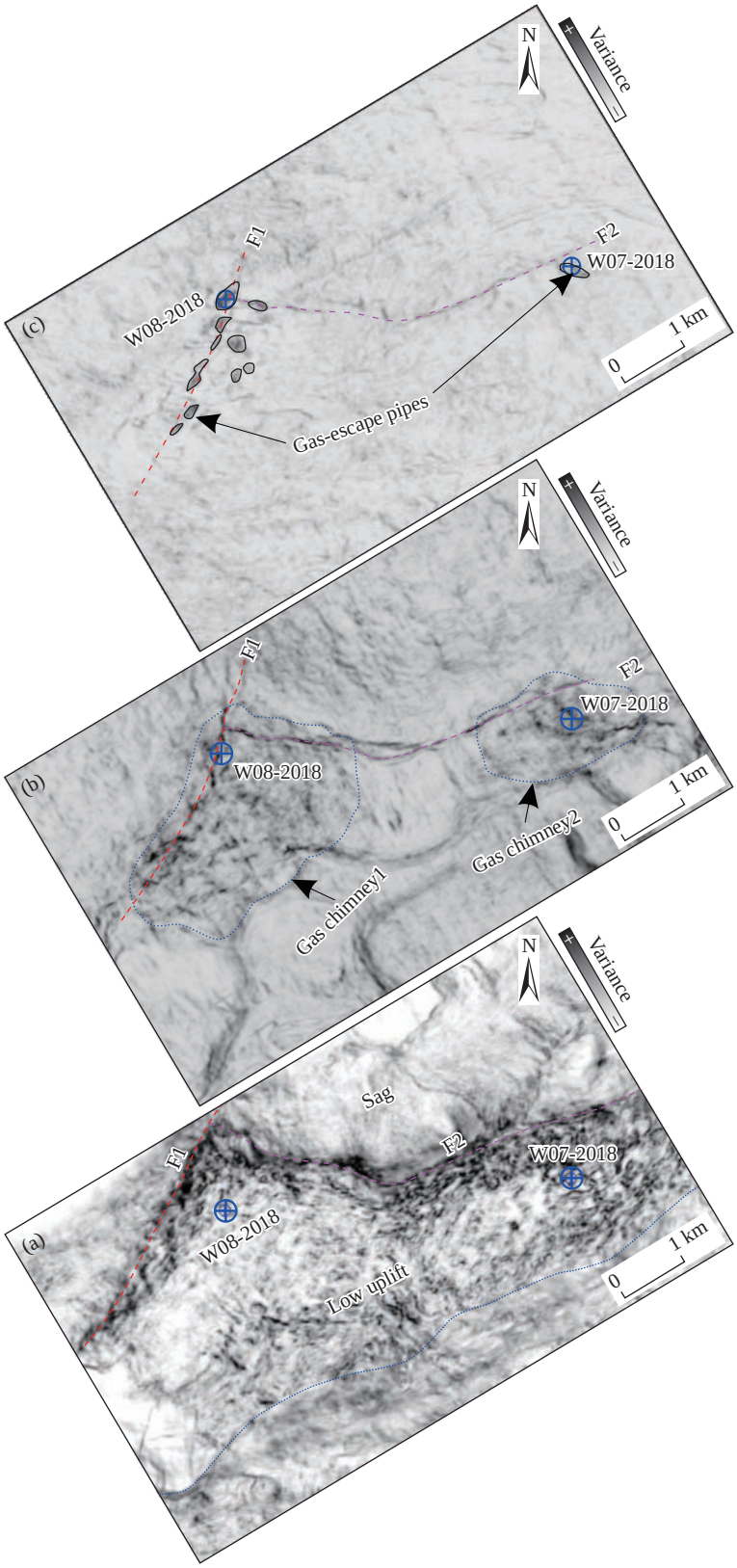

Fig. 4. Variance horizonal slices of spatial ralationship between deep faults and low uplift (3500 ms) (a), gas chimneys (2900 ms) (b), and gas-escape pipes (2450 ms) (c) .

accompanied by high amplitude and low velocity anomalies, as well as scattering, attenuation, and transmission artifacts (Fig. 5). The chimneys form highly vertical columnar zones, with burial depths ranging approximately from 140 mbsf to 800 mbsf. The gas chimney at Site W08-2018 has a plane area of 8.5 km^2, while Site W07-2018 encompasses a gas chimney with a plane area of 5.5 km^2 in the horizontal variance slices (Fig. 5b). The distribution range of gas chimney broadly

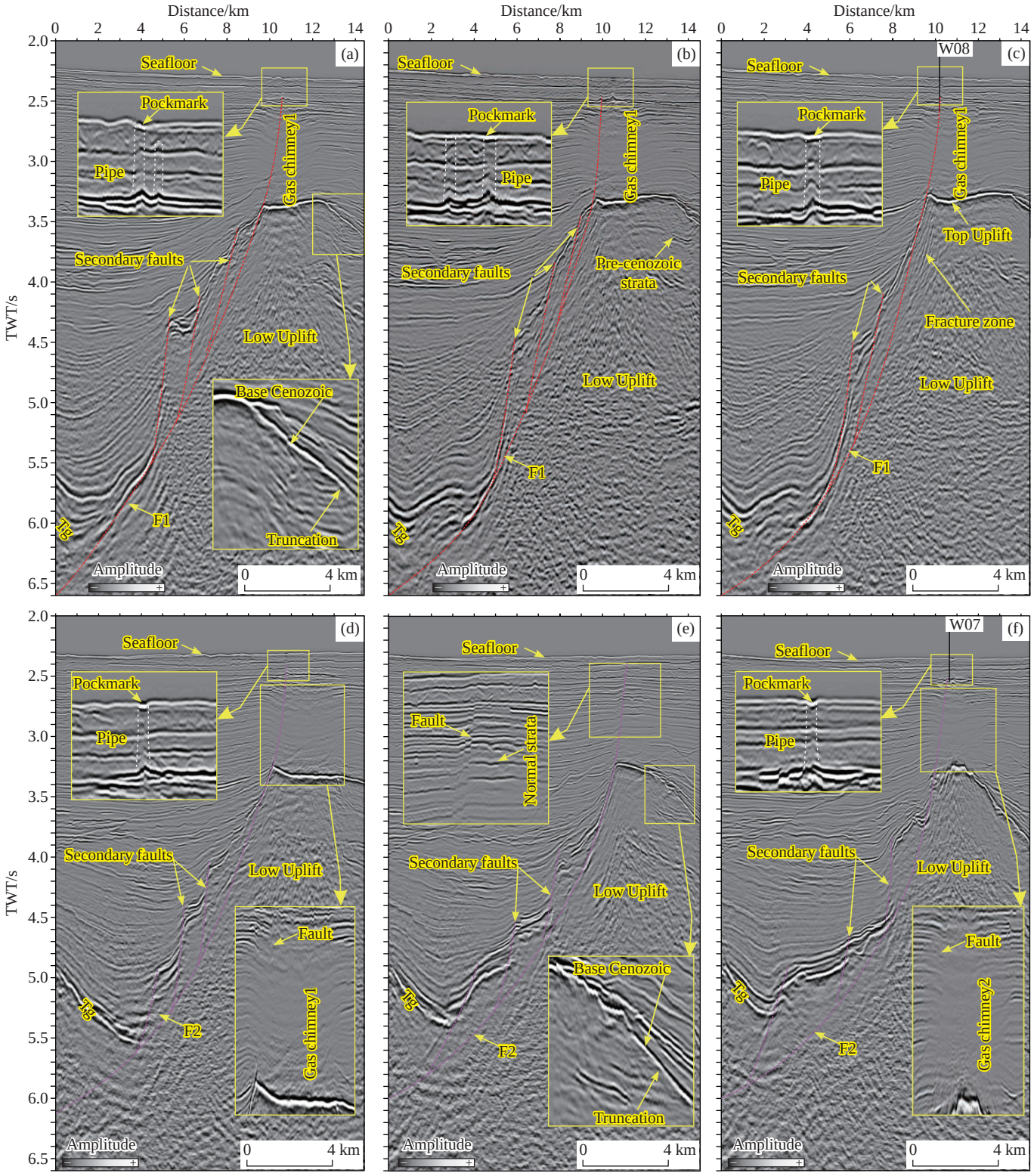

Fig. 5. Typical seismic sections, showing spatial ralationship between deep faults, gas chimneys and pipes, indicating two natural gas hydrate systems. These sections pass through western F1 (a), middle F1 (b), eastern F1 (c), western F2 (d), middle F1 (e) and eastern F1 (f). The location of the sections is shown in the Fig. 1c. Typical angular unconformities are observed in the sections a, b, and e. The red fault is Fault F1 and the pink fault is Fault F2. Gas chimney 1 and gas chimney 2 lied in the western and eastern Fault F2. Seepage pipes and pockmark are developed at the top of the deep faults in sections a, b, c, d, and f.

aligns with areas exhibiting high amplitude anomalies indicative of associated free gas. These chimneys are rooted at the top of the low uplift, and their terminus is marked by mass-transport complexes displaying chaotic seismic reflection configurations. The sedimentary strata traversed by these gas chimneys consist of homogeneous fine-grained argillaceous deposits, characteristic of bathyal-abyssal facies with semi-consolidated to unconsolidated state.

In variance horizontal slices, the gas chimney presents continuous high-value anomalies compared with the same layers outside the chimney in the host succession. Furthermore, the gas chimney is situated in the footwall of the fault and distributed along the fault root (Fig. 5b). In the middle of the gas chimney, it is traversed by the fault. At the top of the gas chimney, high-amplitude seismic reflections were observed, which were subsequently confirmed through drilling to arise from the coexistence of SII hydrate and methane gas in deep-water turbidite sedimentary formations (Wei JG et al., 2021).

4.4. Occurrence of gas hydrate in the gas-escape pipes

Gas-escape pipes primarily intersect the deposits of the multi-stage MTDs sedimentary successions, where the GHSZ is located. The internal geometry manifests in seismic data as vertically stacked reflection discontinuities and consistently upward stratum deformation. These features are attributed to an increase of formation velocity and a reduction in seismic wave propagation time (Figs. 6, 7). The velocity pull-up artifacts may be associated with the accumulation of hydrate and /or carbonate rocks within the pipes.

Horizontal variance slices were used to identify sharp margins and define the horizontal cross-sectional geometry of pipes. Ten elliptical pipes distributed along the regional fault were identified at the top of gas chimney 1. The long axis of these pipes aligns with the strike of the fault, suggesting a close relationship between their formation and the tectonic activity of the regional fault. Three pipes are approximately circular and are located on the hanging wall of the fault, potentially linked to the local structure highs at the top of the gas chimney.

Site W08-2018 was drilled in the middle of the largest gas-escape pipe, which is located at the intersection of faults F1 and F2. Massive carbonate deposits were found between 0 mbsf and 9 mbsf, and massive, layered, nodular and other morphologies of seepage gas hydrates were imaged intermittently between 9 mbsf and 174 mbsf from the X-CT images of the pressure cores (Deng W et al., 2021). The resistivity, acoustic velocity and bulk density of gas hydrate increase in logging data.

The Site W07-2018 was drilled by LWD and coring on the edge of a pipe at the eastern end of the fault F2, which is located on top of the gas chimney 2. Two hydrate intervals were found in the shallow strata of the borehole. This pipe, exhibiting an ellipse shape with a long axis in the northwest direction, is not located inside the fault core, but rather at a structural high point on the top of gas chimney in the footwall of the fault. The heterogeneity of fracture-filling hydrates is obvious. Laterally, hydrates accumulate in the storage space within gas-escape pipes and adjacent sediment, and hydrates of a certain thickness are difficult to gather without pipes connecting to the GHSZ (Figs. 6, 7). Vertically, hydrate occurrence and saturation also show differences between the top and bottom of mass transport deposits (Figs. 6, 7).

5. Discussion

5.1. Influence of deep-large faults on the distribution of gas chimneys

Focused free gas flow is likely attributed to highly-concentrated hydrate in venting systems. The gas composition, gas chromatography and methane isotopes

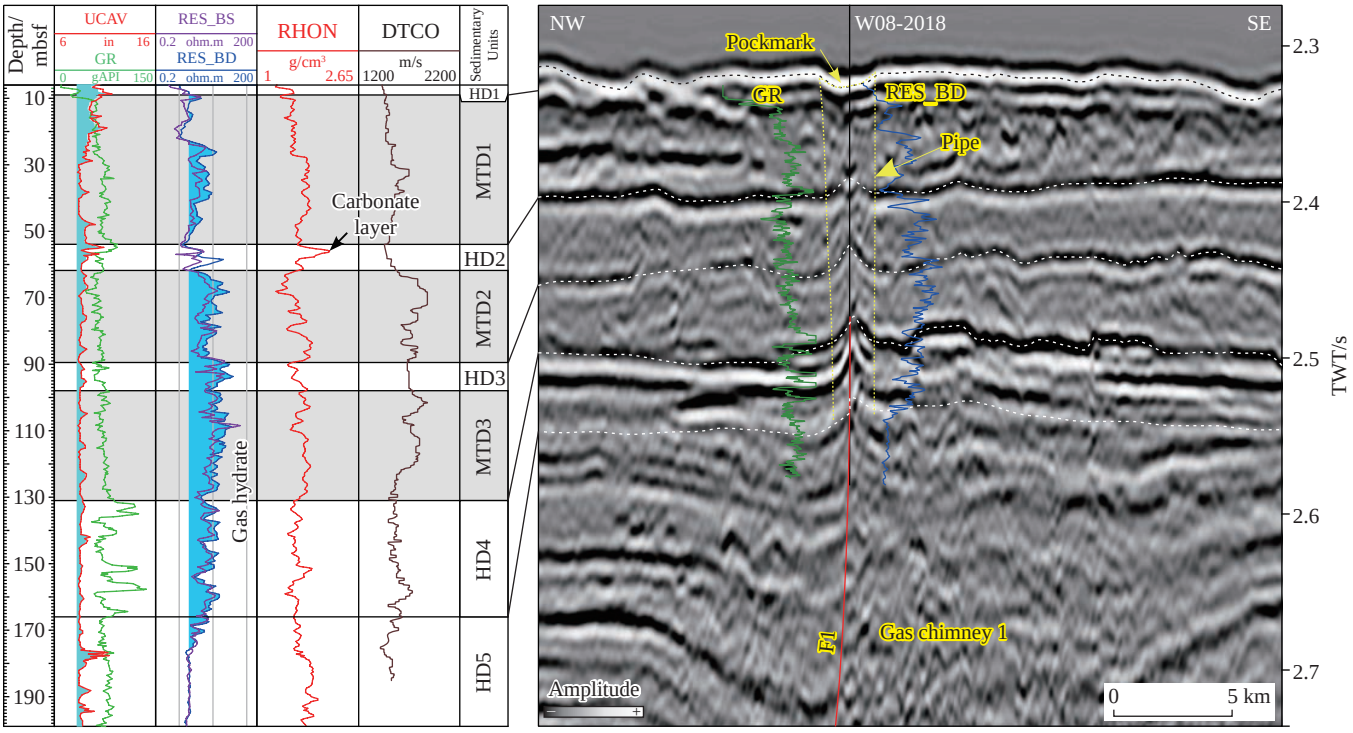

Fig. 6. LWD logs and seismic response characteristics of gas hydrates in the central of the pipe structure at Site W08-2018. MTD is mass transport deposits, HD is hemipelagic deposits.

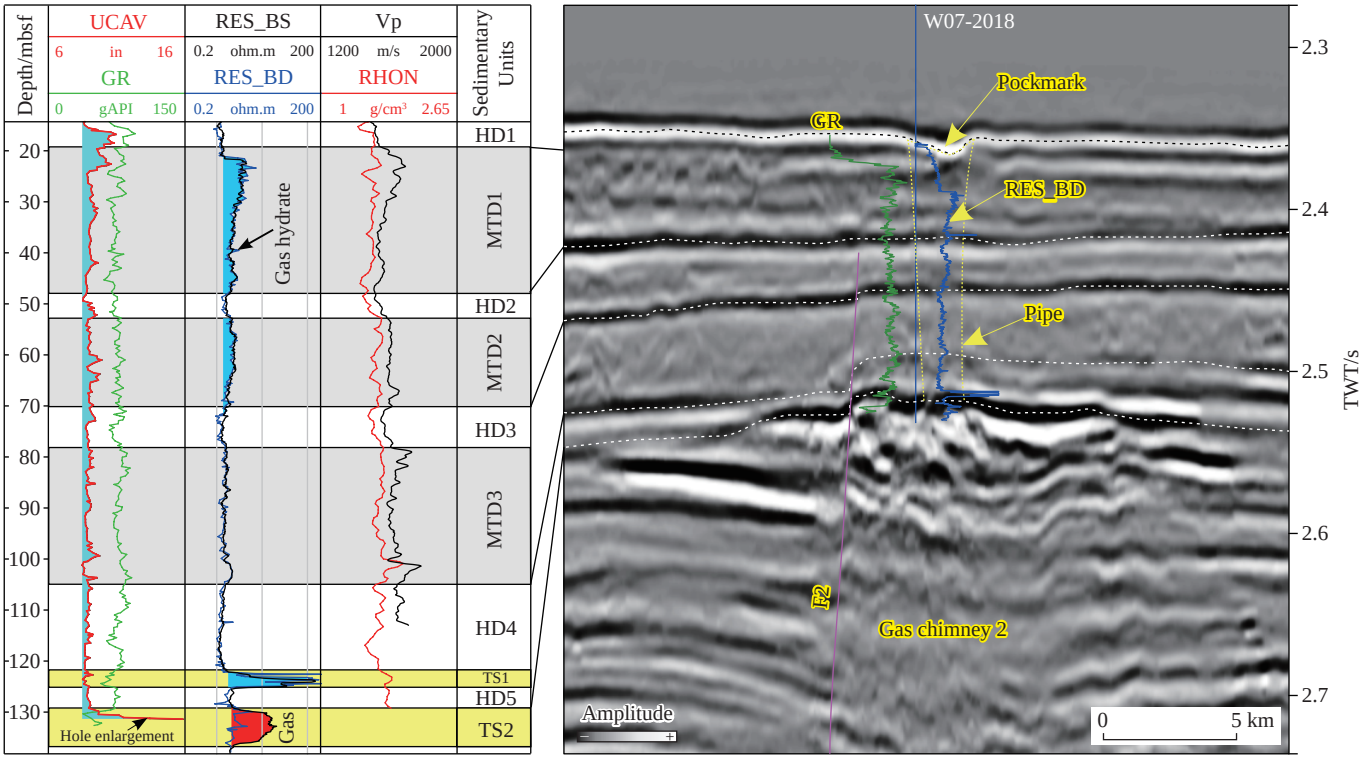

Fig. 7. LWD logs and seismic response characteristics of gas hydrates on the edge of the pipe structure at Site W07-2018. MTD is mass transport deposits, HD is hemipelagic deposits.

suggest that the gas source of concentrated hydrate at Sites W08-2018 in the central QDNB is the mixed contribution of shallow biogenic gas beneath the base of GHSZ and deep thermogenic gas from Early Oligocene coal-measure (Ye JL et al., 2019; Lai HF et al., 2021). The biogenic gas was generated from the Late Miocene-Pliocene silty clay layer at a depth of 2150–2750 m, where the formation temperature was between 35°C and 75°C (Lai HF et al. 2021). The biogenic gas was concentrated toward the fault-controlled anticline and then was transported to the base of GHSZ.

Integrated study from characteristics of fluid inclusions, burial history and thermal evolution showed that the main period of hydrocarbon accumulation in Miocene reservoir was 1.9 Ma–1 Ma in the Ledong-Lingshui Sag of QDNB (Gao Y et al. 2021). Gas filling of L25 Gas Field in Ledong Sag of QDNB occurred around 2.0 Ma and at present, respectively (Zhang YZ et al. 2019). This leads to the speculation that that the primary period of thermogenic gas filling could occur at the last phase of the deep-large faults in the accelerated subsiding period of Songnan Low Uplift.

The upward migration process of deep-seated thermogenic gas to the base of GHSZ may be divided into two stages. In the first stage, gas migrates along the fault and dipping permeable layers in consolidated strata from gas generation center to the top of the low uplift. In the second stage, high-angle vertical migration occurs within gas chimneys in the medium-unconsolidated strata from the top of low uplift to the base of GHSZ.

The thermogenic gas preferentially migrates along the dominant pathways formed by the deep-seated faults and dipping permeable layers, concentrating toward the buried-hill structural closures on the top of the low uplift (Figs. 8, 9). As shown in Fig. 8, two types of dominant migration pathways are observed in the fault system of fault F1 and fault F2. The first type is the dispersal migration pathway formed by concave fault F1, where gas migrates upward along both ends of the fault, supplying gas to gas chimney 1 and gas chimney 2.

The second type is the focusing migration pathway formed at the convex intersection of Faults F1 and F2, where gas converges and supplies to the gas chimney 1 (Fig. 9). The development scale of these dominant migration pathway controls the size of the gas chimney. The size of gas chimney 1 is significantly larger than that of gas chimney 2. Additionally, the migration efficiency of the fluid in the chimney is influenced not only by the size of the chimney, but also by the fluid flux in the chimney. The migration distance of the migration pathways on the east side of the Fault F2 is 3.5 km with a dip angle of 45°. For Fault F1, the migration distance is 5 km with a dip angle of 35°. On the west side of the Fault F2, the migration distance is 5.5 km with a dip angle of 30°.

Obviously, the shorter the migration distance and the larger dip angle of the fault, the less the fluid dissipation occurs in the process of fluid migration, eventually resulting in more fluid migrate to the gas chimney. Therefore, the favorable conditions for the formation of gas chimney 2 are short migration distance and large fault slope angle. However, comparing the distance and angle of pathways, the authors also find that the formation of gas chimney 1 are convergent migration pathways. Therefore, the authors speculate that

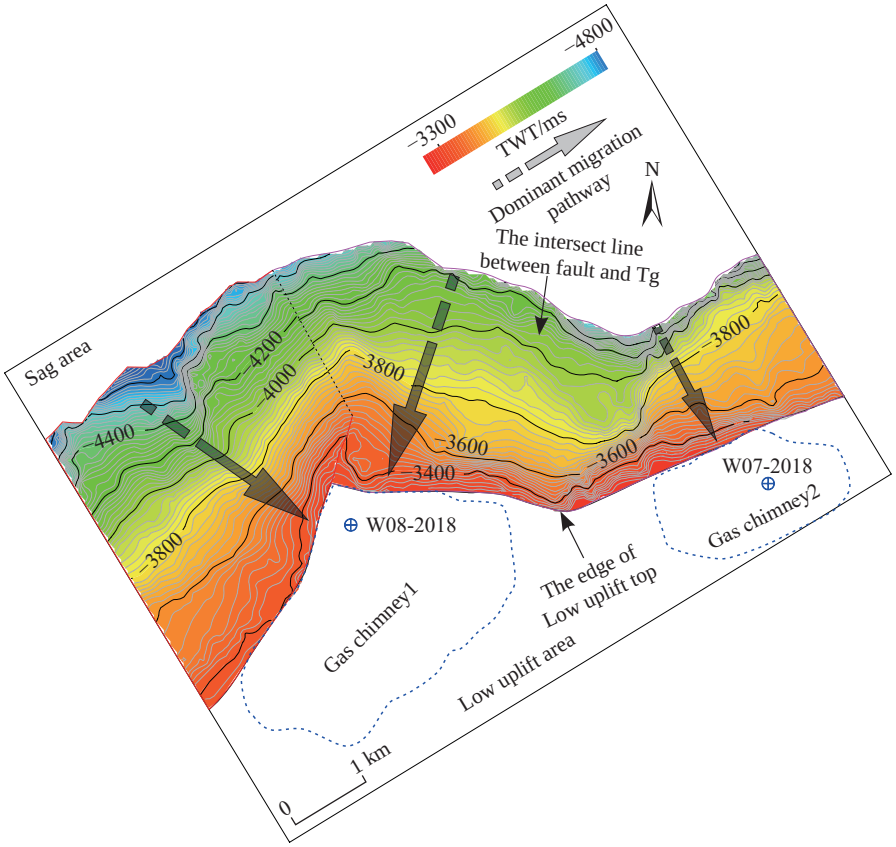

Fig. 8. TWT Contour map of Fault F1 and F2 section showing the dominant migration pathways from thermogenic gas generation zone to the top of low uplift. Two gas chinmeys are situated in footwall of the section of the Fault F1 and F2.

Type	Fault section model	Fault section parameters		Gasaccumulation and pipe-forming
Dispersal	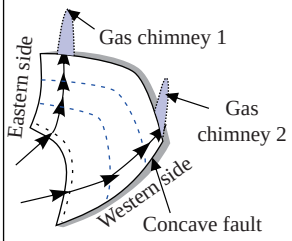	Eastern side	Migration distance: 2.5 km Fault angle: 45°	Part gas was supplied to gas chimney 1 and horizontal area of the gas chimney 2 is 3.0 km^2 One gas conduit was developed at the eastern side of F2
		Western side	Migration distance: 5.5 km Fault angle: 30°	Part gas was supplied to gas chimney 1 One gas pipe was developed at the western side of F2
Focusing	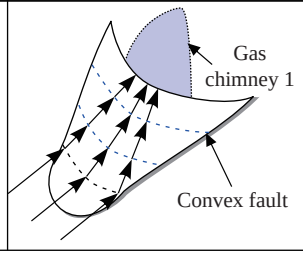	Migration distance: 5–5.5 km Fault angle: 30–35°		Horizontal area of the chimney 1 is 8.5 km^2 Several pipes were developed along fault F1 The largest pipe was developed at the intersection area of fault F1 and F2 (Site W08-2018)

Fig. 9. Migration and accumulation pattern of thermogenic gas along the fault plane. The dominant migration pathways of the convex fault plane have the tendency for concentration and are conducive to the formation of large-scale gas chimney. The dominant migration pathways of the concave fault plane have the tendency for dilution and can only form small-scale gas chimney at the both ends of the fault.

sufficient gas charging and accumulation on top of the low uplift is a prerequisite for gas chimney occurrence, as the episodic expulsion of hydrocarbon from deep gas kitchens of the basin is commonly characterized by high energy and rapid migration.

The formation of gas chimneys results from overpressure gas migration (Bello A et al., 2017). Heggland R (2005) proposed two types of gas chimney based on drilled traps in the Norwegian sector of the North Sea. Type I chimneys serves as hydrocarbon migration pathway and exhibit a narrow feather-like feature on the hanging wall of fault. Type II chimneys cover a wide area at the top of the structure

closure and appear to be unrelated to faults. However, gas chimneys in this study area are situated at the footwall of regional faults and cover a large area on top of low uplift. They may be associated seal failure on the top of this structural closure and hydrocarbon leakage of the buried-hill gas traps.

The Seal failure of the structural closure may be the result of the fracture network induced by sustained disequilibrium compaction on both sides of the low uplift. In the east of our study, a buried-hill gas reservoir (YL8-3) was successfully drilled, confirming that buried-hill traps on low uplift have good gas accumulation potential (Yang JH et al., 2019). Thus, large-scale hydrocarbon leakage may be derived from overpressure within the buried-hill gas reservoir sourced by thermogenic gas charging and accumulation. In addition, gas chimneys occur in highly layered, clay-dominated, and semi-unconsolidated to unconsolidated marine sedimentary successions without significant lateral fluid transport within, resulting from hydraulic fracturing of 'seal' units above the overpressure source trap (Fig. 10).

5.2. Influence of deep-large faults on the distribution of the gas-escape pipes

The venting gas hydrate system in Site W08-2018 and W07-2018 is mainly developed in focused gas-escape pipes within muddy mass transport deposits (Figs. 6, 7). The spatial distribution of pipe structures is considered critical in providing leakage pathways and determining the geological occurrences of the venting gas hydrates (Fig. 10). These pipes are hypothesized to consist of a network of interconnected fractures oriented sub-vertically or radially (Bull JM et al., 2018), allowing for cross-stratal, pressure-driven fluid through the hydrate stability zone. Such pipe structures are characterized by high resistivity and P wave velocities (Figs. 6, 7).

Two principal mechanisms have been suggested to explain pipe formation, including hydraulic fracturing and capillary invasion (Cartwright J and Santamarina C, 2015). Hydraulic fracturing may serve as an initiator to pipe formation with gas propagating upward through newly formed fractures and

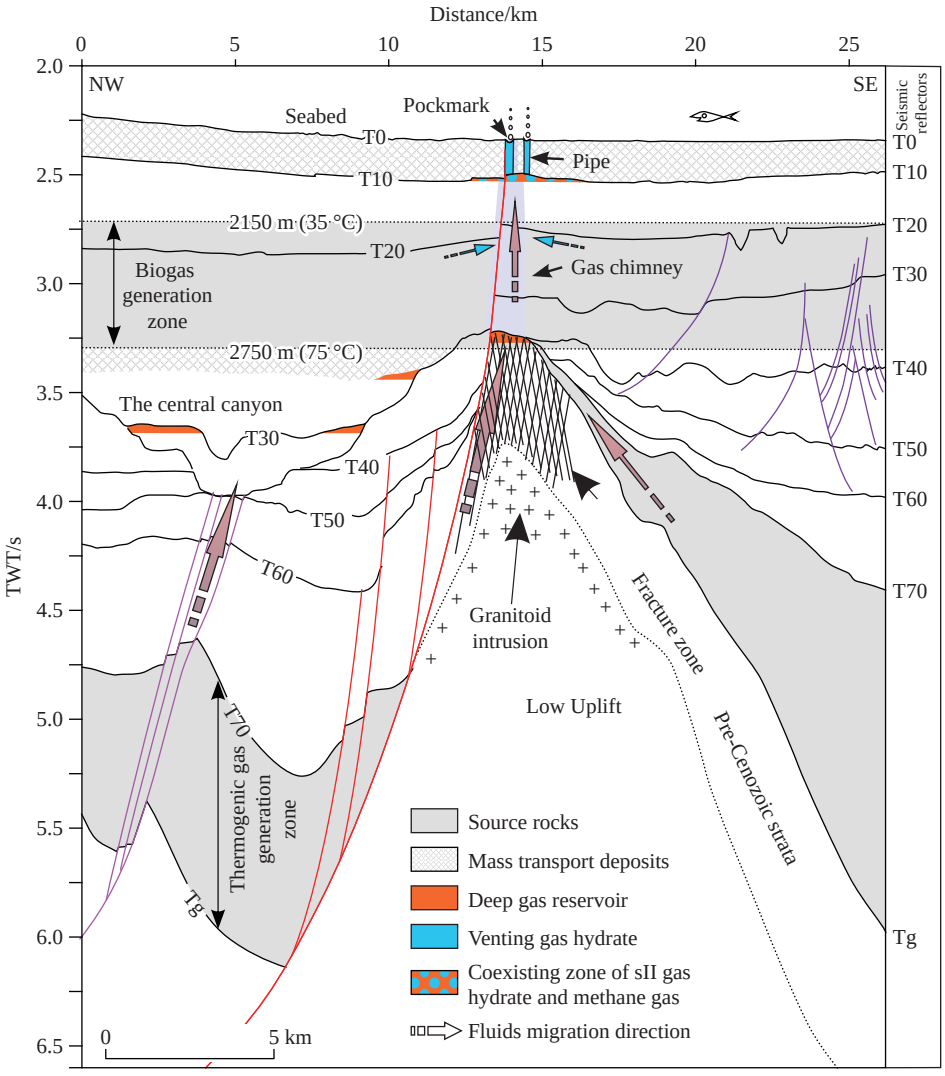

Fig. 10. Schematic diagram showing the migration and accumulation of gas-bearing fluids along the deep fault on the low uplift and gas chimney. Also showing the forming model of the venting gas hydrate system within the gas-escape pipes at the top of gas chimney (afterYe JL et al., 2019).

reactivated pre-existing fractures in fine-grained sediment (Cevatoglu M et al., 2015; Roche B et al., 2021). The process is often followed by flow localization and erosive fluidization, particularly if overpressure within the underlying high permeability reservoirs builds up due to the gas buoyancy (Callow B et al., 2021). This can lead to the formation of seafloor pockmarks at the pipe terminus (Figs. 6, 7). When gas encounters strata with high heterogeneity, these processes can be augmented by capillary effects related to gas phase accumulations, gas exsolution, and expansion (Cartwright J and Santamarina C, 2015).

The authors observe that two types of pipe structures were developed at the apices of gas chimneys. One type is located at the top of the deep faults (Fig. 6), which is related to the reactivation of deep-large faults. The other type is located at the highest points of BSRs (Fig. 7), which is connected with the buildup of pore pressure due to reduced permeability and subsequent hydrofracturing. Further study is needed to reconstruct the pressure conditions responsible for the formation of gas escape pipes. It is worth noting that most of pipe structures in the study area are distributed along deep-large regional faults, indicating that the reactivation of deep-large faults plays a significant role to influences the distribution of the gas-escape pipes (Fig. 4). This further emphasizes the influence of deep-large faults on the gas hydrate system in the Songnan Low Uplift.

5.3. Implications for the gas migration process associated with the deep faults

The venting gas hydrate system often contains concentrated hydrates that fill fractures in muddy sediments and is formed by focused free gas beneath the base of GHSZ (You KH et al., 2019). Building on the insights gained from the influence of deep-large faults on the distribution of gas chimneys and pipe structures presented in this study, the authors propose a model (Fig. 10) that subdivides the accumulation process of focused free gas into three stages: stages I, II, and III.

Stage I is characterized by migration and accumulation of deeply-generated thermogenic gases towards a granite buried-hill reservoir at the crest of the Songnan Low Uplift. The dominant migration pathways are controlled by the regional faults within the deep consolidated stratigraphic units of the basin (Figs. 8, 9).

In the Stage II, leakage towards the GHSZ occurs via a cross-stratal advection process from the gas reservoir at the crest of the Songnan Low Uplift. The relationship between gas chimneys and the distribution of the shallow gas-bearing amplitude anomalies in this study suggests that the dominant migration pathways are mainly controlled by gas chimneys. Fluid migration along the regional faults may occur only during their activity within the semi-consolidated or unconsolidated stratigraphic units of the basin. Therefore, the authors suppose that the large-scale gas chimneys may be related to hydrocarbon leakage derived from overpressure within the buried-hill gas reservoir. During this stage, thermogenic, secondary microbial and microbial gas were mixed in the gas chimneys and were migrated vertically into the bottom of mass transport deposits.

In the Stage III, pipe structures and fracture-filling hydrates form. The rate of methane release from the gas chimney is a significant factor in the formation of methane hydrates in inclined formations (Bei KQ et al., 2022). Additionally, in inclined formations, gas pressure beneath the GHSZ or mass transport deposits can exceed the least principal stress of the overburden (Meazell PK and Flemings PB, 2022), leading to the creation of pipe structures and driving focused gas flow into the GHSZ to form fracture-filling hydrates. In this process, the reactivation of deep-large faults facilitates free gas flow into the GHSZ, contributing to the formation of fracture‐filling hydrates.

Overall, this model suggests that the presence of deep-large faults significantly influences the migration and accumulation of gas, which in turn impacts the formation of gas hydrates. This study suggest that it is important to consider the influence of hydrocarbon migration process for the gas hydrate formation in future gas hydrate exploration.

6. Conclusions

Based on high-precision 3D seismic and LWD data, the authors have investigated the relationship between the venting gas hydrate distribution and regional deep-large faults at the margin of the Songnan Low Uplift in the middle QDNB. The following conclusions are obtained:

(i) Two deep-large faults, F1 and F2, develop on the margin of the Songnan Low Uplift, extending all the way to the seabed. The activity and reactivity of the faults can be divided into four phases: Regional extension during the rifting stage, rapid activity due to magmatic diapir intrusion, activity decreasing and halt during the thermal subsidence, and reactivity caused by differential subsidence during accelerated subsidence.

(ii) The formation of gas chimneys is controlled by the two faults acting as the dominant migration pathways. Gas chimney 1 is primarily formed by convergent fluid migration resulting from the intersection of two faults. The formation of gas chimneys may be relevant to the leakage of deep over-pressured gas reservoir, the tensile flexure deformation caused by sustained disequilibrium compaction on the low uplift, and the weak lateral diffusion of late Miocene to Pliocene fine-grained muddy deposits. Therefore, the gas chimney 2 benefits from a steeper fault plane and shorter migration distance.

(iii) The geometry and distribution of pipe structures are influenced by the reactivity of the two faults, which facilitate free gas to migrate across the GHSZ. Most of gas-escape pipes originate underneath mass transport deposits and terminate at a seafloor pockmark with authigenic carbonate. These gas-escapes pipes penetrate clay-dominated mass transport deposits and gas hydrates accumulate in a network of hydraulic fractured zone within them.

CRediT authorship contribution statement

Jin-Feng Ren, Hai-Jun Qiu and Zeng-Gui Kuang conceived of the presented idea. All authors discussed the results and contributed to the final manuscript.

Declaration of competing interest

The authors declare no conflicts of interest.

Acknowledgement

This research was jointly supported by the National Natural Science Foundation of China (42376221, 42276083), Director Research Fund Project of Guangzhou Marine Geological Survey (2023GMGSJZJJ00030), National Key Research and Development Program of China (2021YFC2800901), Guangdong Major Project of Basic and Applied Basic Research (2020B030103003), and the project of the China Geological Survey (DD20230064). The authors are grateful for all participants of the China National Gas Hydrate Drilling Expedition (GMGS8).

References

Bei KQ, Tian HL, Xu TF, Li YP, Yin, ZY. 2022. Effects of key geological factors in the long-term transport of CH_4 and the CH_4-hydrate formation behavior with formation dip. Journal of Natural Gas Science and Engineering, 103, 104615. doi: 10.1016/j.jngse.2022.104615.

Bello A, Heggland R, Peacock DCP. 2017. Pressure significance of gas chimneys. Marine and Petroleum Geology, 86, 402–407. doi: 10.1016/j.marpetgeo.2017.06.005.

Berndt C,Chi WC, Jegen M, Lebas E, Crutchley, G, Muff S, Hölz S, Sommer M, Lin S, Liu, CS, Lin A, Klaeschen D, Klaucke I, Chen LW, Hsu HH., Kunath P, Elger J, McIntosh K, Feseker T. 2019. Tectonic controls on gas hydrate distribution off SW Taiwan. Journal of Geophysical Research: Solid Earth, 124, 1164–1184. doi:10.1029/2018JB016213.

Boswell R, Collett TS. 2011. Current perspectives on gas hydrate resources. Energy and Environmental Science, 4, 1206–1215. doi: 10.1039/C0EE00203H.

Bull JM, Berndt CB, Minshul, TM, Henstock T, Bayrakci G, Gehrmann R, Provenzano G, Bottner C, Schramm B, Callow B, Best AI. 2018. Constraining leakage pathways through the overburden above sub-seafloor CO_2 storage reservoirs. In: 14th Greenhouse Gas Control Technologies Conference Melbourne 21–26 October 2018 (GHGT–14).

Burwicz E, Rüpke LH, Wallmann K. 2011. Estimation of the global amount of submarine gas hydrates formed via microbial methane formation based on numerical reaction-transport modeling and a novel parameterization of Holocene sedimentation. Geochimica et Cosmochimica Acta, 75(16), 4562–4576. doi: 10.1016/j.gca.2011.05.029.

Callow B, Bull JM, Provenzano G, Böttner C, Birinci H, Robinson AH, Henstock TJ, Minshull TA, Bayrakci G, Lichtschlag A. 2021. Seismic chimney characterisation in the North Sea–Implications for pockmark formation and shallow gas migration. Marine and Petroleum Geology, 133, 105301. doi: 10.1016/j.marpetgeo.2021.105301.

Cartwright J, Santamarina C. 2015. Seismic characteristics of fluid escape pipes in sedimentary basins: Implications for pipe genesis. Marine and Petroleum Geology, 65, 126–140. doi: 10.1016/j.marpetgeo.2015.03.023.

Cevatoglu M, Bull JM, Vardy ME, Gernon TM, Wright IC, Long D. 2015. Gas migration pathways, controlling mechanisms and changes in sediment acoustic properties observed in a controlled sub-seabed CO_2 release experiment. International Journal of Greenhouse Gas Control, 38, 26–43. doi: 10.1016/j.ijggc.2015.03.005.

Collett TS, Johnson A, Knapp C, Boswell R. 2009. Natural gas hydrates: A review. In Collett TS, Johnson A, Knapp C, Boswell R (Eds.), Natural gas hydrates-Energy resource potential and associated geologic hazards, AAPG Memoir, Vol. 89, 146–219.

Collett TS. 2004. Gas hydrates as a future energy resource. Geotimes, 49(11), 24–27.

Deng W, Liang JQ, Zhang W, Kuang ZG, Zhong T, He YL. 2021. Typical characteristics of fracture-filling hydrate-charged reservoirs caused by heterogeneous fluid flow in the Qiongdongnan Basin, northern south China sea. Marine and Petroleum Geology, 124, 104810. doi: 10.1016/j.marpetgeo.2020.104810.

Dhakal S, Gupta I. 2021. Simulating Gas Hydrate Formation in the Southern Hydrate Ridge, Cascadia Margin. Journal of Natural Gas Science and Engineering, 88, 103845. doi: 10.1016/j.jngse.2021.103845.

Freire AFM, Matsumoto R, Santos LA. 2011. Structural-stratigraphic control on the Umitaka Spur gas hydrates of Joetsu Basin in the eastern margin of Japan Sea. Marine and Petroleum Geology, 28. 1967–1978. doi: 10.1016/j.marpetgeo.2010.10.004.

Gao Y, Qu XY, Yang XB, You L, Zhong J, Dong XF, Cao YQ, Wang YP. 2021. Characteristics of Fluid Inclusions and Accumulation Period of Miocene Reservoir in Ledong-Lingshui Sag of Qiongdongnan Basin. Marine Origin Petroleum Geology, 23(1), 83–90 (in Chinese with English abstract). doi: 10.3969/j.issn.1672-9854.2018.01.010.

He JX, Ning ZJ, Zhao B, Wan ZF, Meng DJ. 2022. Preliminary analysis and prediction of the strategic replacement area for gas hydrate exploration in the South China Sea. Earth Science, 47(5), 1549–1568 (in Chinese with English abstract). doi: 10.3799/dqkx.2021.119.

He YL, Liang JQ, Kuang ZG, Deng W, Ren JF, Lai HF, Meng MM, Zhang W. 2022. Migration and accumulation characteristics of natural gas hydrates in the uplifts and their slope zones in the Qiongdongnan Basin, China. China Geology, 5(2), 234–250. doi: 10.31035/cg2022004.

Heggland R. 2005. Using gas chimneys in seal integrity analysis: A discussion based on case histories. In: Boult P, Kaldi J (Eds.), Evaluating Fault and Cap Rock Seals. AAPG, Hedberg Series, 2, 237–245. doi: 10.1029/2018JB016213.

Koh DY, Kang H, Lee JW, Park Y, Kim SJ, Lee J, Lee JY, Lee H. 2016. Energy-efficient natural gas hydrate production using gas exchange. Applied Energy, 162, 114–130. doi: 10.1016/j.apenergy.2015.10.082.

Kvenvolden KA. 1995. A review of the geochemistry of methane in natural gas hydrate. Organic Geochemistry, 23, 997–1008. doi: 10.1016/0146-6380(96)00002-2.

Lai HF, Fang YX, Kuang ZG, Ren JF, Liang JQ, Lu JA, Wang GL, Xing CZ. 2021. Geochemistry, origin and accumulation of natural gas hydrates in the Qiongdongnan Basin, South China Sea: Implications from site GMGS5-W08. Marine and Petroleum Geology, 123, 104774. doi: 10.1016/j.marpetgeo.2020.104774.

Lee MW, Collett TS. 2013. Characteristics and interpretation of fracture‐filled gas hydrate–An example from the Ulleung Basin, East Sea of Korea. Marine and Petroleum Geology, 47, 168–181. doi: 10.1016/j.marpetgeo.2012.09.003.

Liang J, Zhang Z, Lu J, Guo Y, Sha Z, Su PB, Zhang W. 2021. Characterization of gas accumulation at a venting gas hydrate system in the Shenhu area, South China Sea. Interpretation, 9(2), SD1–SD14. doi: 10.1190/INT-2020-0105.1.

Liang JQ, Zhang W, Lu JA, Wei JG, He YL. 2019. Geological occurrence and accumulation mechanism of natural gas hydrates in the eastern Qiongdongnan Basin of the South China Sea: insights from site GMGS5-W9-2018. Marine Geology, 418, 106042. doi: 10.1016/j.margeo.2019.106042.

Liang QY, Hu Y, Feng D, Peckmann J, Chen LY, Yang SX, Liang JQ, Tao J, Chen DF. 2017. Authigenic carbonates from newly discovered active cold seeps on the northwestern slope of the South China Sea: Constraints on fluid sources, formation environments, and seepage

dynamics. Deep Sea Research Part I: Oceanographic Research Papers, 124, 31–41. doi: 10.1016/j.d sr.2017.04.015.

Liang C, Liu C, Xie X, Yu X, He YL, Su M, Chen H, Zhou Z, Tian DM, Mi HG, Li MJ, Zhang H. 2021. Basal shear zones of recurrent mass transport deposits serve as potential reservoirs for gas hydrates in the Central Canyon area, South China Sea. Marine Geology, 441(4), 106631. doi: 10.1016/j.margeo.2021.106631.

Mao KN, Xie XN, Xie YH, Ren JY, Chen H. 2015. Post-rift tectonic reactivation and its effect on deep-water deposits in the Qiongdongnan Basin, northwestern South China Sea. Marine Geophysical Research, 36 (2), 227–242. doi: 10.1007/s11001-015-9248-x.

Malinverno A. 2010. Marine gas hydrates in thin sand layers that soak up microbial methane. Earth and Planetary Science Letters, 292, 399–408. doi: 10.1016/j.epsl.2010.02.008.

Matsumoto R, Tanahashi M, Kakuwa Y, Snyder G, Ohkawa S, Tomaru H, Morita S. 2017. Recovery of thick deposits of massive gas hydrates from gas chimney structures, eastern margin of Japan Sea. Fire in the Ice, 17(1), 1–6.

Meazell PK, Flemings PB. 2022. The evolution of seafloor venting from hydrate-sealed gas reservoirs. Earth and Planetary Science Letters, 579, 117336. doi: 10.1016/j.epsl.2021.117336.

Milkov AV. 2004. Global estimates of hydrate-bound gas in marine sediments: How much is really out there? Earth-Science Reviews, 66(3–4), 183–197. doi: 10.1016/j.earscirev.2003.11.002.

Paganoni M, King JJ, Foschi M, Mellor-Jones K, Cartwright JA. 2019. A natural gas hydrate system on the Exmouth plateau (NW shelf of Australia) sourced by thermogenic hydrocarbon leakage. Marine and Petroleum Geology, 99, 370–392. doi: 10.1016/j.marpetgeo.2018.10.029.

Ren JF, Cheng C, Xiong PF, Kuang ZG, Liang JQ, Lai HF, Chen ZG, Chen Y, Li T, Jiang T. 2022. Sand-rich gas hydrate and shallow gas systems in the Qiongdongnan Basin, northern South China Sea. Journal of Petroleum Science and Engineering, 215, 110630. doi: 10.1016/j.petrol.2022.110630.

Roche B, Bull JM, Marin-Moreno H, Leighton T, Falcon-Suarez IH, White PR, Provenzano G, Tholen M, Lichtschlag A, Li J, Faggetter M. 2021. Time-lapse imaging of CO_2 migration within near-surface sediments during a controlled subseabed release experiment. International Journal of Greenhouse Gas Control, 109, 103363. doi: 10.1016/j.ijggc.2021.103363.

Ryu BJ, Collett TS, Riedel M, Kim GY, Chun JH, Bahk JJ, Lee JY, Kim HH, Yoo DG. 2013. Scientific results of the Second Gas Hydrate Drilling Expedition in the Ulleung Basin (UBGH2). Marine and Petroleum Geology, 47, 1–20. doi: 10.1016/j.marpetgeo.2013.07.007.

Santra M, Flemings PB, Heidari M, You KH. 2022. Occurrence of high-saturation gas hydrate in a fault compartmentalized anticline and the importance of seal, Green Canyon, abyssal northern Gulf of Mexico: AAPG Bulletin, 106, 5, 981–1003. doi: 10.1306/08182120149.

Sha Z, Liang J, Zhang G, Yang S, Lu J, Zhang Z, McConnell DR, Humphrey G. 2015. A seepage gas hydrate system in northern South China Sea: Seismic and well log interpretations. Marine Geology, 366, 69–78. doi: 10.1016/j.margeo.2015.04.006.

Shi HS, Yang JH, Zhang YZ, Gan J, Yang JH. 2019. Geological understanding innovation and major breakthrough to natural gas exploration in deep water in the Qiongdongnan Basin. China Petroleum Exploration, 24(6), 691–698. doi: 10.3969/j.issn.1672-7703.2019.06.001.

Sloan ED, Koh C. 2007. Clathrate hydrates of natural gases. Boca Raton, FL: CRC Press, 45–102.

Sloan ED. 2003. Fundamental principles and applications of natural gas hydrates. Nature, 426, 353–359. doi: 10.1038/nature02135.

Song P. 2021. Shallow migration and accumulation systems in the deep-water areas of the Qiongdongnan basin and their control on natural gas hydrate accumulation. Marine Geology Frontiers, 37(7), 11–21 (in Chinese with English abstract). doi: 10.16028/j.1009-2722.2021.088.

Torres ME, Wallmann K, Trehu AM, Bohrmann G, Borowski WS, Tomaru H. 2004. Gas hydrate growth, methane transport, and chloride enrichment at the southern summit of Hydrate Ridge, Cascadia margin off Oregon. Earth and Planetary Science Letters, 226, 225–241. doi: 10.1016/j.epsl.2004.07.029.

Trèhu AM, Long PE, Torres ME, Bohrmann G, Rack FR, Collect TS, Goldberg DS, Milkov AV, Riedel M, Schultheiss P. 2004. Three‐dimensional distribution of gas hydrate beneath southern Hydrate Ridge: Constraints from ODL Leg 204. Earth and Planetary Science Letters, 222(3–4), 845–862. doi: 10.1016/j.epsl.2004.03.035.

Wallmann K, Pinero E, Burwicz E, Haeckel M, Hensen C, Dale A, Ruepke L. 2012. The global inventory of methane hydrate in marine sediments: A theoretical approach. Energies, 5(7), 2449. doi: 10.3390/en5072449.

Wei JG, Wu TT, Zhu LQ, Fang YX, Liang JQ, Lu HA, Cai WJ, Xie ZY, Lai PX, Cao J, Yang TB. 2021. Mixed gas sources induced co-existence of sI and sII gas hydrates in the Qiongdongnan Basin, South China Sea. Marine and Petroleum Geology, 128, 105024. doi: 10.1016/j.marpetgeo.2021.105024.

Xiong XF, Guo XX, Zhu JT, Guo MG, Li X. 2019. Causes of natural gas geochemical differences in the deep water area gas field, western South China Sea. Natural Gas Geoscience, 30(7), 1−1053, 1062 (in Chinese with English abstract). doi: 10.11764/j.issn.1672-1926.2019.04.010.

Xu SL，You L，Mao XL，Zhong J, Wu SJ. 2019. Reservoir Characteristics and Controlling Factors of Granite Buried Hill in Songnan Low Uplift, Qiongdongnan Basin. Earth Science, 44(8), 2717–2728 (in Chinese with English abstract). doi: 10.3799/dqkx.2019.186.

Yang JH, Huang BJ, Yang JH. 2019. Gas accumulation conditions and exploration potentials of natural gases in Songnan Low Uplift, deep water area of Qiongdongnan Basin. China Offshore Oil and Gas, 31(2), 1–10. doi: 10.11935/j.issn.1673-1506.2019.02.001.

Ye JL, Wei JG, Liang JQ, Lu JA, Lu HL, Zhang W. 2019. Complex gas hydrate system in a gas chimney, South China Sea. Marine and Petroleum Geology, 104, 29–39. doi: 10.1016/j.marpetgeo.2019.03.023.

Yoo DG, Kim KJ, Kang NK, Yi BY, Cho MH. 2017. Plio-Quaternary seismic stratigraphy and depositional history of the Ulleung Basin, East Sea: Association with debris-flow activity. Quaternary International, 459, 69–88. doi: 10.1016/j.quaint.2017.06.040.

You K, Flemings PB, Malinverno A, Collett TS, Darnell KN. 2019. Mechanisms of methane hydrate formation in geological system. Reviews of Geophysics, 57, 1146–1196. doi: 10.1029/2018RG000638.

Zhang CM, Wang ZF, Sun Z, Sun ZP, Liu JB, Wang ZW. 2013. Structural differences between the western and eastern Qiongdongnan Basin: evidence of Indochina block extrusion and South China Sea seafloor spreading. Marine Geophysical Research, 34(3), 309–323. doi: 10.1007/s11001-013-9187-3.

Zhang W, Liang JQ, Lu JA, Meng MM, He YL, Seng W, Feng JX. 2020. Characteristics and controlling mechanism of typical leakage gas hydrate reservoir forming system in the Qiongdongnan Basin, northern South China Sea. Natural Gas Industry, 40(8), 90–99 (in Chinese with English abstract). doi: 10.3787/j.issn.1000-0976.2020.08.007.

Zhang YZ, Li XS, Xu XD, Gan J, Yang XB, Liang G, He XH, Li X. 2019a. Genesis, origin, and accumulation process of the natural gas of L25 Gas Field in the western deep-water area, Qiongdongnan Basin. Marine Origin Petroleum Geology, 24(03), 1–10 (in Chinese with English abstract).

Zhang YZ, Xu XD, Gan J, Yang XB, Zhu JT, Yang JH, He XH, Guo XX. 2019b. Formation condition and accumulation of Pliocene strata-trapped gas field L18 in the deepwater area of the Qiongdongnan Basin. Haiyang Xuebao, 41(3), 121–133 (in Chinese with English abstract). doi: 10.3969/j.issn.0253-4193.2019.03.012.

Zhu JT, Deng Y, Guo MG. 2020. Mineralization conditions and accumulation pattern of the gas hydrate in Qiongdongnan Basin Floor Plain. China Offshore Oil and Gas, 32(3), 10–19 (in Chinese with English abstract).